Double-Notch Frequency-Coded Corner Reflectors for sub-THz chipless RFID Tags

Jesús Sánchez-Pastor, Ahmed Kamel, Martin Schüßler, Rolf Jakoby, Alejandro Jiménez-Sáez

***Abstract*—Frequency-coded corner reflectors (CR) have been proposed as an essential component of chipless indoor localization systems at sub-terahertz frequencies. These tags operate by encoding a notch in the frequency domain of the otherwise stable backscattered power spectrum by a CR. The current state-of-the-art in the WR-3 band (220 GHz to 330 GHz) is based on single notch frequency selective surfaces (FSS), whose maximum number of implementable frequency codes is too few for indoor localization applications. This work proposes the coding of the CR with a single layer FSS implementing two notches, using split ring resonators (SRRs) with two different resonance frequencies. The concept is demonstrated by encoding the response of a 3-cm-edge CR with an FSS resonating at 242 GHz and 308 GHz. The tag achieves a maximum radar cross-section (RCS) of 3 dBsqm at 275 GHz. Four more tags are demonstrated by simply varying the radii of the SRRs. It is estimated that this approach can implement up to 15 non-overlapping codes within the WR-3 band, three times more than the state-of-the-art.**

***Index Terms*—Frequency selective surfaces, indoor localization, chipless radio-frequency identification (RFID), sub-THz.**

I. Introduction

Corner reflectors (CRs) have been considered as chipless RFID tags in multiple applications within the mm-wave frequency range, due to their low complexity and well-known and large backscattered response. For example, they are found in works dealing with smart environments [1], [2], maritime [3] and unmanned aerial vehicles applications [4] and automotive radar [5], [6], to name a few. Particularly in the case of indoor self-localization, sub-THz (100 GHz to 300 GHz) systems present a good trade-off between microwave's deep penetration capabilities through non-metallic materials and the fine spatial and time resolution of the optical frequency range, resulting in millimeter positioning accuracy [7] [8], while enabling non-line of sight applications [9], [10].

Current state-of-the-art frequency coded CR as tags in sub-THz indoor localization systems include employing dielectric resonator arrays [11], [12], one dimensional photonic crystals [13] or frequency selective surfaces (FSS) [14]. All of them encode a notch in the backscattered power of an otherwise flat response of a CR. In the specific case of FSS-based tags, a stop band structure placed in the aperture of a CR does not allow its resonance frequency (f_{res}) to propagate *into* the CR. Thus, its f_{res} is scattered away, while the rest of the signal spectrum allowed to go through is backscattered in the direction of arrival by the CR. This is perceived as a notch in the received signal level [14].

The aforementioned tags operate within the W-band (75 GHz to 110 GHz), with tags based on dielectric resonator arrays and FSSs having been recently verified as a part of an indoor synthetic aperture radar system , achieving positioning accuracy in the millimeter range [15]. However, only FSSs have been demonstrated up to the upper sub-THz range (WR-3, from 220 GHz to 330 GHz), due to their easiness of fabrication via lithography-based processes [16], whereas the other structures still present significant challenges in terms of manufacturing complexity at this frequency band. Further, the work in [16] features only one notch with a 20 GHz bandwidth in the tag's frequency response, which restricts the number of codes implementable within the WR-3 band to 5, limiting the suitability of such tags in a real indoor environment, where a minimum of 10 tags are needed for accurate 3D localization [12].

This work proposes a tag concept able to implement up to 15 frequency codes, by leveraging a two-notch FSS. Each notch is implemented in a single layer by split ring resonators (SRRs) with different f_{res}, arranged in a rectangular lattice.

II. Single-layer double-notch frequency selective surface

FSSs operating at sub-THz and THz frequencies are already present in literature, but they either operate at only one f_{res} [17], [18], or their higher order f_{res} lie beyond the WR-3 band [19]–[22], requiring a complete re-design of the FSSs. Further, the f_{res} of the FSS should be stable for interrogation angles (θ) of approximately $\pm 45°$, to achieve a stable frequency response of the tag. In this regard, FSSs whose period is smaller than the operating wavelength feature a more stable f_{res} for varying θ [23]–[25].

Split ring resonators (SRRs) [26]–[28] are a possibility to achieve a miniaturized unit cell due to their compact size. Furthermore, gaps are implemented within the ring, which increase the total capacitance of the structure, hence further miniaturizing it for a specific f_{res}. Depending on the gap orientation, the SRR resonates for Transverse Electric (TE), Transverse Magnetic (TM) plane waves or both of them. For this work, a single gap is implemented on the "bottom" of the SRRs, limiting their excitation to TM polarization.

The substrate employed to implement the FSS is Rogers RT 5880 with a relative permittivity ε_{r} of 2.28 and loss

Manuscript received xxxxxx; revised xxxxx.

This work was funded by the Deutsche Forschungsgemeinschaft (DFG, German Research Foundation) – Project-ID 287022738 – TRR 196 MARIE within project C09. *(Corresponding author: Jesús Sánchez-Pastor.)*

All authors are with the Institute of Microwave Engineering and Photonics, Technische Universität Darmstadt, 64289 Darmstadt, Germany. (E-mail, in order: jesus.sanchez@tu-darmstadt.de; ahmed.kamel@stud.tu-darmstadt.de; schuessler@imp.tu-darmstadt.de; jakoby@imp.tu-darmstadt.de; alejandro.jimenez_saez@tu-darmstadt.de)

Digital Object Identifier xxxxxxxxxxx

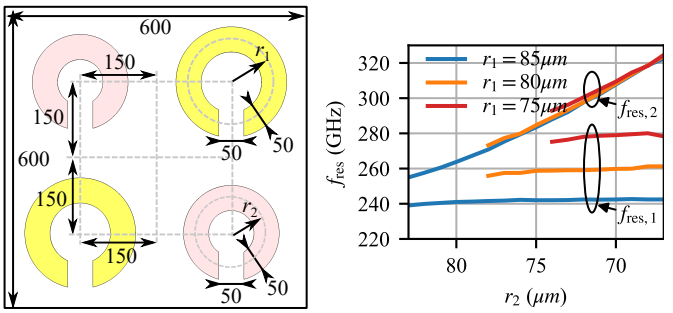

(a) (b)

Fig. 1. **(a)** Sketch of the simulated unit cell, presenting the dimensions for the SRRs. All units are in µm, while the SRRs with different f_{res} are colored differently. **(b)** Simulated f_{res} in dependence of r_1 and r_2.

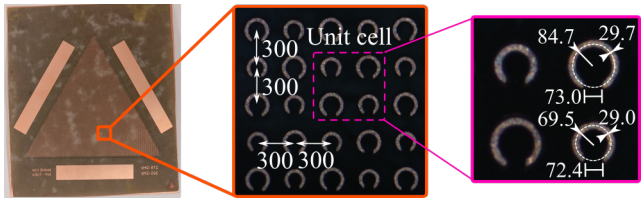

Fig. 2. Manufactured FSS with f_{res} at approximately 242 GHz and 308 GHz. The inset shows a zoom in the structure. All units are in µm.

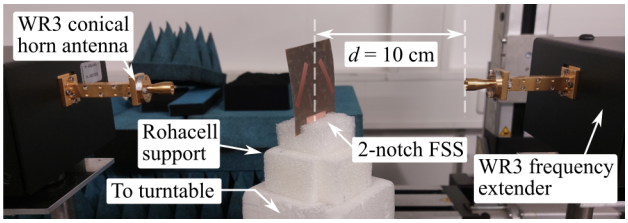

(a)

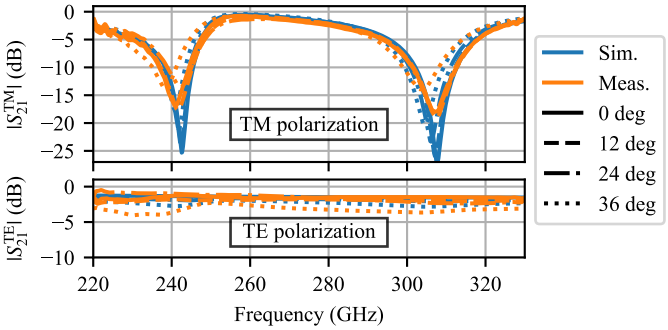

(b)

Fig. 3. **(a)** Measurement setup to characterize the S_{21} of the FSS. **(b)** Comparison between simulated and measured S_{21} for different θ and TM (top) and TE (bottom) plane waves. The results are normalized to the free space path, i.e., without the FSS placed in the setup.

tangent $\tan(\delta)$ of 0.002 at 300 GHz [29]. The copper thickness is 18 µm, which limits the minimum feature size to approximately 50 µm. Since the FSS is manufactured with a wet chemical etching process, thinner line widths might lead to a complete undercut of the copper layer [30]. The unit cell of the double-notch FSS is presented in Fig. 1a, where the two different SRRs are arranged in a rectangular pattern and interleaved, with the target of both decreasing and homogenizing inter-element cross-coupling, so the f_{res} of each SRR can be independently chosen by simply varying its radius.

The FSS is simulated for TE and TM plane waves employing the frequency domain solver from CST Studio Suite, with unit cell boundaries. Its f_{res} are presented in Fig. 1b, where it is shown that two f_{res}, corresponding to each resonator, are controllable by individually varying the radius of each ring. Henceforth, the radii chosen are $r_1 = 85\,\mu m$ and $r_2 = 70\,\mu m$, corresponding to f_{res} of approximately 242 GHz and 308 GHz, respectively.

The manufactured FSS is presented in Fig. 2, along with its dimensions, measured with an optical microscope. First, the FSS is designed in a triangular shape with the same edge length as the CR (3 cm), as it is intended to cover its aperture. This results in 2181 repetitions of the unit cell presented in Fig. 1a. Second, it is noticeable that the ring's dimensions are different from the design ones. Mainly, the rings are narrower, decreasing from a width of 50 µm to ≈ 29 µm, and the gaps are wider, increasing from 50 µm to ≈ 73 µm, due to the wet etching process employed for its manufacturing.

The setup shown in Fig. 3a is used to measure the transmission coefficient of the FSS (S_{21}), where the FSS is placed between two 21 dBi gain WR-3 horn antennas connected to a Vector Network Analyzer (Agilent Technologies N5222A) and two Virginia Diodes WR-3 extensions. A turntable is used to analyze the angle-dependent FSS response, while multiple reflections between the antennas are filtered out using a rectangular time window between 0.1 ns to 1.1 ns.

The results for selected angular rotations are presented in Fig. 3b for both TM and TE polarizations, compared to simulations. The measurements corresponding to TM plane waves present the two expected notches at approximately 242 GHz and 308 GHz, corresponding to the f_{res} of each implemented SRR. The maximum measured f_{res} shift between $\pm 36°$ is -3.5 GHz ($-1.22\,\%$) for the higher f_{res}, which matches the simulated value, of $-1\,\%$. The results for larger θ are masked by cross-coupling between the horn antennas, and thus not considered. Regardless, the FSS presents a stable frequency behavior that allows its use as a coding structure for the CR-based tags. Finally, as expected due to the gap position, no resonance is present for the TE polarization, where the S_{21} oscillates between -1 dB to -3 dB.

III. Double-Notch Frequency-Coded Corner Reflectors

The FSS is cut in a triangular shape and fixed to a CR with adhesive tape to conform the tag. To characterize its performance, the tag is placed at a distance of 200 cm to one horn antenna, like a monostatic radar setup, as presented in Fig. 4. The measured reflection coefficient (S_{11}) is filtered in the time-domain using a rectangular window between 13.4 ns to 15 ns. This allows for both filtering out environmental clutter and the structural mode of the tag, which is received for θ close to frontal incidence. For larger θ, the reflection on the FSS (main cause for the structural mode) is scattered away from the transmitting/receiving antenna.

The tag's measured S_{11}, along with a comparison with the uncoded CR, is presented in Fig. 5a for TM plane waves,

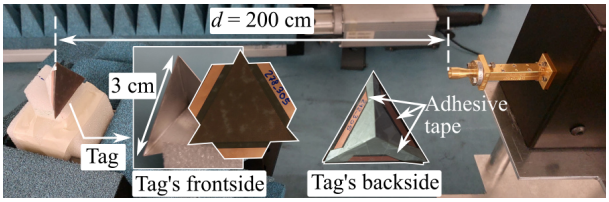

Fig. 4. Setup to measure the tag's σ. The inset shows the CR employed, along with the cut FSS that is placed on its aperture. The FSS is bent along the thick copper lines present on its sides, which are also employed to affix it to the CR with adhesive tape.

as this polarization is the only one that presents a resonance. First, the two notches corresponding to the SRRs with f_{res} at 242 GHz and 308 GHz are clearly appreciable, with a magnitude lower than 10 dB from their surrounding spectrum. Second, the tag's backscattered signal magnitude between 260 GHz to 280 GHz is similar to the CR, owing to the FSS presenting a S_{21} close to 0 dB, as it was presented in Fig. 3.

The radar cross-section (σ) is a quantity that describes the amount of backscattered power by a structure, independent of the measurement setup employed. To estimate the tag's σ, a simple solution is to measure a target whose σ can be calculated analytically, such as a trihedral corner reflector, and then to apply Eq. 1.

$$\frac{\sigma_{\text{tag}}}{\sigma_{\text{reference}}} = \frac{|S_{11,\text{tag}}|^2}{|S_{11,\text{reference}}|^2} \tag{1}$$

In this case, the reference target is the uncoded CR, whose analytical σ varies between 2.6 dB m^2 at 220 GHz to 6.1 dB m^2 at 330 GHz.

The measured σ for both TE and TM polarizations and $\pm 50°$ is presented in Fig. 5b as a heatmap, where brighter colors represent a larger measured σ and vice versa. The graph clearly shows both the lack of resonance for the TE polarization and the two stable notches present at 242 GHz and 308 GHz for the TM polarization, corresponding to the frequency code of the tag.

IV. Discussion

Following the results in Fig. 5b, the σ_{tag} at 275 GHz is of 3 dB m^2, whereas the analytical σ_{CR} is 4.5 dB m^2 at this frequency. I.e., the FSS introduces a loss of 1.5 dB. This loss in σ decreases the maximum range at which the tag response can be received compared to an uncoded CR. The monostatic radar range equation (Eq. 2) is employed to calculate the maximum distance at which the tag could be detected with our setup.

$$R_{\text{max}} = \sqrt[4]{\frac{P_{\text{t}} G^2 \lambda^2 \sigma}{(4\pi)^3 S_{\text{min}}}} \tag{2}$$

In Eq. 2, G accounts for the antenna gain (21 dBi), P_{t} stands for transmitted power (0 dBm) and S_{min} describes the minimum received power needed at the receiver. This value includes the noise floor of the equipment (−90 dB), as well as a minimum out-of-resonance signal-to-noise ratio, which [7], [12], [31], [32] propose to be set to at least 10 dB to achieve an almost errorless ranging and identification. Thus, S_{min} is

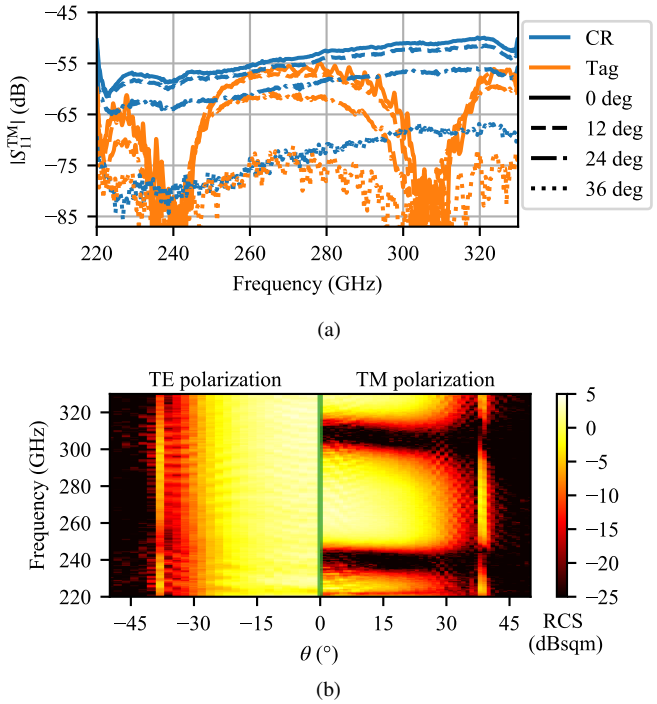

Fig. 5. **(a)** Comparison of the measured S_{11} for the CR and its frequency-coded counterpart for TM polarization and different θ. **(b)** Heatmap depicting the measured σ of the tag for TE (left) and TM (right) polarizations between $\pm 50°$. Only half of the angular response is shown for each polarization, as the σ has a symmetric response centered at 0° for both of them.

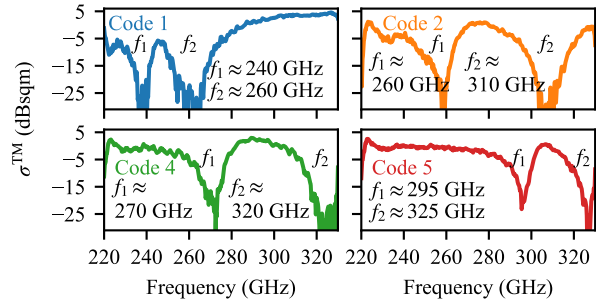

Fig. 6. Measured $\sigma(\theta = 10°)$ for four additional tags with different frequency codes operating in the WR-3 band. Codes are named following the corresponding FSS number in Tab. I.

set to −80 dB. With these values, the maximum distance up to which the uncoded CR and the tag can be detected at 275 GHz are 7.2 m and 6.6 m (8 % decrease), respectively.

To pursue a multi tag scenario, different frequency codes (different f_{res}) can be implemented by selecting other radii for the SRRs. To show this principle, four additional tags are implemented by varying r_1 and r_2 between 85 µm and 70 µm, and their measured σ is presented in Fig. 6. For all tags, the two notches are clearly appreciable within the WR-3 spectrum, even when they are implemented closely together, as it is the case of the tag corresponding to the "code 1", with f_{res} at 240 GHz and 260 GHz. For this tag, the middle frequency between the notches (245 GHz) presents an σ that is 8.5 dB lower than the uncoded CR (−5 dB m^2 and 3.5 dB m^2, respectively), decreasing the maximum readout range to 4.4 m.

Tab. I presents a summary of the design parameters for

TABLE I
SUMMARY OF THE FIVE DESIGNED AND MANUFACTURED FSSS FOR THE CODING OF CRS

	SRR 1									SRR 2								
	r (µm)		w (µm)		g (µm)		f_{res} (GHz)			r (µm)		w (µm)		g (µm)		f_{res} (GHz)		
FSS	sim.	meas.	sim.	meas.	sim.	meas.	sim.	sim. adj.	meas.	sim.	meas.	sim.	meas.	sim.	meas.	sim.	sim. adj.	meas.
1	85	84.23	50	32.22	50	66.91	241.01	252.01	239.01	80	80.12	50	29.11	50	67.28	263.78	273.13	263.00
2	85	84.86	50	31.80	50	74.59	242.11	256.19	256.62	75	74.51	50	30.50	50	74.28	283.69	301.84	305.82
3	85	84.73	50	29.70	50	72.98	242.22	257.07	240.99	70	69.48	50	28.98	50	72.40	307.78	324.83	307.36
4	80	79.07	50	26.58	50	74.51	259.71	278.08	268.31	70	69.54	50	25.53	50	75.15	308.11	328.35	318.85
5	75	74.39	50	26.61	50	73.42	279.18	296.78	289.00	70	69.45	50	27.62	50	73.11	309.54	326.15	328.57

TABLE II
COMPARISON OF SUB-THZ FREQUENCY-CODED CORNER REFLECTORS

Ref.	Coding	Freq. range (GHz)	B_{notch} (GHz)	m	N_{notch}	s	$\sigma_{\mathrm{CR}}/\sigma_{\mathrm{tag}}$ (dB)
This work[1]	**FSS, SRRs**	**220 - 330**	**20**	**5**	**2**	**15**	**1.5**
[16][1]	FSS, cross dipole	220 - 330	20	5	1	5	< 0.5
[14][1]	FSS, cross dipole	75 - 110	7	5	1	5	< 0.5
[12]	Dielectric resonator array	75 - 110	3.2	10	1	10	< 0.5
[11][2]	Dielectric resonator array	75 - 110	7	5	2	15	-
[13][2]	1D photonic crystal	75 - 110	17	2	1	2	< 0.5

[1] Only TM polarization considered.
[2] Not a trihedral CR, but a dihedral one.

each FSS and their dimensions measured with an optical microscope, as well as their measured and simulated f_{res} before (sim.) and after (sim. adj.) accounting for variations due to the manufacturing process. The FSS that was presented in Section II is underlined in gray. It is noteworthy the difference between the designed ring widths and gaps ($50\,\mu\mathrm{m}$ each) and the manufactured ones, of the order of $30\,\mu\mathrm{m}$ and $70\,\mu\mathrm{m}$, respectively, due to the manufacturing process. The maximum deviation between the adjusted simulations and the measured f_{res} is $6.3\,\%$, which is attributed to the optical microscope used, in which the resolution was of $1\,\mu\mathrm{m/px}$, and to the manual measurement of the dimensions. As established in [33], a more accurate characterization achieves a better match between the adjusted simulations and measurements.

The addition of a second notch in the FSS allows for the increase in the number of frequency codes (s) implementable within a certain bandwidth, which can be estimated as

$$s = \sum_{i=1}^{N_{\mathrm{notch}}} \binom{m}{i} \tag{3}$$

Where m is the number of slots implementable within a certain frequency range, dependent on the minimum bandwidth required for each notch, B_{notch}. This value is dependent on both the notch bandwidth and the f_{res} shift regarding θ.

Tab. II presents a comparison of state-of-the-art sub-THz frequency-coded CRs. Do note that s is calculated assuming no overlap between the B_{notch} of two different codes, so the maximum number of 15 distinguishable tags is a conservative estimate, which could be increased by allowing notch overlap such as in [34]. First, the two tags that operate in the upper part of the sub-THz spectrum ($220\,\mathrm{GHz}$ to $330\,\mathrm{GHz}$) employ FSSs, due to their simplified manufacturing complexity. Second, the tag presented in this work can implement up to 15 signatures within the WR-3 band, trice as much as the previous state-of-the-art [16] at this frequency range, and of the order of / greater than other W-band works, which feature either two notches [11] or photonic crystal cavities with narrower resonance bandwidths [13]. Third, one drawback of the approach presented in this work is the aforementioned $1.5\,\mathrm{dB}$ loss in σ_{tag}, compared to the CR. The other publications showcased in Tab. II do not present this issue, owing to either coding only one f_{res} in the FSS [14], [16] or using dielectric resonators with narrow resonance bandwidths [11]–[13].

V. CONCLUSION

This work has presented the development of single-layer, 2-notch frequency selective surfaces (FSS) as coding structures for corner reflectors (CR) employed as sub-THz chipless tags. The FSSs are based on stop band split ring resonators (SRR) , which present a resonance for TM plane waves. The performance of one tag with resonance frequencies (f_{res}) at $242\,\mathrm{GHz}$ and $308\,\mathrm{GHz}$ has been described in terms of radar cross-section (σ), where it was found that it presents a decrease of $8\,\%$ in the maximum readout range ($6.6\,\mathrm{m}$) compared to its uncoded CR counterpart ($7.2\,\mathrm{m}$), due to non-ideal outside-of-resonance transmission through the FSS. To showcase the possibility of implementation of multiple tags, five different FSSs are designed by varying the radii of the SRRs. This approach can implement up to 15 codes, three times more than the previous state-of-the-art.

As an outlook, it is possible to profit from the other side of the substrate to implement two further SRRs, provided that inter-element cross coupling is decreased, so each resonator has an independently controllable f_{res}. To achieve so, the manufacturing technology employed should be able to accurately achieve metal line widths and gaps of the order of $5\,\mu\mathrm{m}$ to $10\,\mu\mathrm{m}$. This development could increase the number of achievable codes up to 30, provided that the decrease in the outside-of-resonance σ remains within acceptable levels.

ACKNOWLEDGMENTS

This work was funded by the Deutsche Forschungsgemeinschaft (DFG, German Research Foundation) – Project-ID 287022738 – TRR 196 MARIE within project C09.

REFERENCES

[1] K. Kelevitz, T. J. Wright, A. J. Hooper, and S. Selvakumaran, "Novel Corner-Reflector Array Application in Essential Infrastructure Monitoring," *IEEE Geosci. Remote Sens. Lett.*, vol. 60, pp. 1–18, 2022.

[2] X. Yang, J. Sayono, and Y. Zhang, "CubeSense++: Smart Environment Sensing with Interaction-Powered Corner Reflector Mechanisms," ser. UIST '23. New York, NY, USA: Association for Computing Machinery, 2023. [Online]. Available: https://doi.org/10.1145/3586183.3606744

[3] J. Stastny, S. Cheung, G. Wiafe, K. Agyekum, and H. Greidanus, "Application of RADAR Corner Reflectors for the Detection of Small Vessels in Synthetic Aperture Radar," *IEEE J. Sel. Topics Appl. Earth Observ. Remote Sens.*, vol. 8, no. 3, pp. 1099–1107, 2015.

[4] T. Iizuka, T. Sasatani, T. Nakamura, N. Kosaka, M. Hisada, and Y. Kawahara, *MilliSign: MmWave-Based Passive Signs for Guiding UAVs in Poor Visibility Conditions*. New York, NY, USA: Association for Computing Machinery, 2023.

[5] W.-J. Liao, Y.-C. Hou, C.-C. Tsai, T.-H. Hsieh, and H.-J. Hsieh, "Radar Cross Section Enhancing Structures for Automotive Radars," *IEEE Antennas Wireless Propag. Lett.*, vol. 17, no. 3, pp. 418–421, 2018.

[6] T. Iizuka, N. Kosaka, M. Hisada, Y. Kawahara, and T. Sasatani, "Trimmed Aperture Corner Reflector for Angle-Selective Chipless RFID," *IEEE Antennas and Wireless Propagation Letters*, vol. 22, no. 10, pp. 2537–2541, 2023.

[7] M. El-Absi, A. Alhaj Abbas, A. Abuelhaija, F. Zheng, K. Solbach, and T. Kaiser, "High-Accuracy Indoor Localization Based on Chipless RFID Systems at THz Band," *IEEE Access*, vol. 6, pp. 54 355–54 368, 2018.

[8] A. Jiménez-Sáez, A. Alhaj-Abbas, M. Schüßler, A. Abuelhaija, M. El-Absi, M. Sakaki, L. Samfaß, N. Benson, M. Hoffmann, R. Jakoby, T. Kaiser, and K. Solbach, "Frequency-Coded mm-Wave Tags for Self-Localization System Using Dielectric Resonators," *Journal of Infrared, Millimeter, and Terahertz Waves*, vol. 41, no. 8, p. 908–925, jun 2020.

[9] T. S. Rappaport, Y. Xing, O. Kanhere, S. Ju, A. Madanayake, S. Mandal, A. Alkhateeb, and G. C. Trichopoulos, "Wireless Communications and Applications Above 100 GHz: Opportunities and Challenges for 6G and Beyond," *IEEE Access*, vol. 7, pp. 78 729–78 757, 2019.

[10] A. Batra, F. Sheikh, M. Wiemeler, D. Göhringer, and T. Kaiser, "Investigation of THz SAR Through-Wall Sensing in Indoor Environment," in *2022 Antenna Measurement Techniques Association Symposium (AMTA)*, 2022, pp. 1–6.

[11] K. Solbach, A. A. Abbas, M. El-Absi, A. Abuelhaija, and T. Kaiser, "Experimental Demonstration of Double-Notch RCS Spectral Signature of Corner Reflector Tag for THz Self-Localization System," in *2020 Third International Workshop on Mobile Terahertz Systems (IWMTS)*, 2020, pp. 1–4.

[12] M. El-Absi, A. Al-Haj Abbas, and T. Kaiser, "Chipless RFID Tags Placement Optimization as Infrastructure for Maximal Localization Coverage," *IEEE Journal of Radio Frequency Identification*, vol. 6, pp. 368–380, 2022.

[13] A. Alhaj Abbas, Y. Zhao, J. C. Balzer, K. Solbach, and T. Kaiser, "Photonic-Crystal-Resonator-Based Corner Reflector With Angle-of-Arrival Sensing," *IEEE Journal of Radio Frequency Identification*, vol. 7, pp. 451–462, 2023.

[14] A. Jiménez-Sáez, M. Schüßler, M. El-Absi, A. A. Abbas, K. Solbach, T. Kaiser, and R. Jakoby, "Frequency Selective Surface Coded Retroreflectors for Chipless Indoor Localization Tag Landmarks," *IEEE Antennas and Wireless Propagation Letters*, vol. 19, no. 5, pp. 726–730, 2020.

[15] A. Batra, A. A. Abbas, J. Sánchez-Pastor, M. El-Absi, A. Jiménez-Sáez, M. Khaliel, J. Barowski, M. Wiemeler, D. Göhringer, I. Rolfes, R. Jakoby, and T. Kaiser, "Millimeter Wave Indoor SAR Sensing Assisted With Chipless Tags-Based Self-Localization System: Experimental Evaluation," *IEEE Sensors Journal*, vol. 24, no. 1, pp. 844–857, 2024.

[16] A. Jiménez-Sáez, *High-RCS Wide-Angle Retroreflective Tags Towards THz*. Cham: Springer International Publishing, 2022, pp. 93–129.

[17] D. S. Wang, B. J. Chen, and C. H. Chan, "High-Selectivity Bandpass Frequency-Selective Surface in Terahertz Band," *IEEE Transactions on Terahertz Science and Technology*, vol. 6, no. 2, pp. 284–291, 2016.

[18] A. Ghavidel, M. Kokkonen, and S. Myllymäki, "A double layer FSS filter for sub-THz applications," *Scientific Reports*, vol. 11, no. 1, Oct. 2021. [Online]. Available: http://dx.doi.org/10.1038/s41598-021-99256-2

[19] Y. Yuan, C. Bingham, T. Tyler, S. Palit, T. H. Hand, W. J. Padilla, N. M. Jokerst, and S. A. Cummer, "A dual-resonant terahertz metamaterial based on single-particle electric-field-coupled resonators," *Applied Physics Letters*, vol. 93, no. 19, p. 191110, 11 2008.

[20] S. Hussain, J. Min Woo, and J.-H. Jang, "Dual-band terahertz metamaterials based on nested split ring resonators," *Applied Physics Letters*, vol. 101, no. 9, p. 091103, 08 2012.

[21] S. Vegesna, Y. Zhu, A. Bernussi, and M. Saed, "Terahertz Two-Layer Frequency Selective Surfaces With Improved Transmission Characteristics," *IEEE Transactions on Terahertz Science and Technology*, vol. 2, no. 4, pp. 441–448, 2012.

[22] S. Qiao, Y. Zhang, Y. Zhao, Y. Zhou, S. Liang, and Z. Yang, "Multiband Frequency-Selective Surface With Five Resonance Peaks in Terahertz Band," *IEEE Transactions on Terahertz Science and Technology*, vol. 6, no. 2, pp. 292–299, 2016.

[23] B. A. Munk, *Frequency Selective Surfaces: Theory and Design*. Nashville, TN: John Wiley & Sons, apr 2000.

[24] S. Ghosh and K. V. Srivastava, "An angularly stable dual-band fss with closely spaced resonances using miniaturized unit cell," *IEEE Microwave and Wireless Components Letters*, vol. 27, no. 3, pp. 218–220, 2017.

[25] T. Hong, W. Xing, Q. Zhao, Y. Gu, and S. Gong, "Single-Layer Frequency Selective Surface With Angular Stability Property," *IEEE Antennas and Wireless Propagation Letters*, vol. 17, no. 4, pp. 547–550, 2018.

[26] P. Gay-Balmaz and O. J. F. Martin, "Electromagnetic resonances in individual and coupled split-ring resonators," *Journal of Applied Physics*, vol. 92, no. 5, pp. 2929–2936, 08 2002.

[27] N. Katsarakis, T. Koschny, M. Kafesaki, E. N. Economou, and C. M. Soukoulis, "Electric coupling to the magnetic resonance of split ring resonators," *Applied Physics Letters*, vol. 84, no. 15, pp. 2943–2945, 04 2004.

[28] K. Aydin and E. Ozbay, "Identifying magnetic response of split-ring resonators at microwave frequencies," *Opto-Electron. Rev.*, vol. 14, no. 3, jan 2006.

[29] X. Ruan and C. H. Chan, "Terahertz free-space dielectric property measurements using time- and frequency-domain setups," *International Journal of RF and Microwave Computer-Aided Engineering*, vol. 29, no. 9, 2019.

[30] O. Çakır, "Review of Etchants for Copper and its Alloys in Wet Etching Processes," in *Optics Design and Precision Manufacturing Technologies*, ser. Key Engineering Materials, vol. 364. Trans Tech Publications Ltd, 2 2008, pp. 460–465.

[31] R.-E.-A. Anee and N. C. Karmakar, "Chipless RFID Tag Localization," *IEEE Transactions on Microwave Theory and Techniques*, vol. 61, no. 11, pp. 4008–4017, 2013.

[32] J. Alam, M. Khaliel, A. Fawky, A. El-Awamry, and T. Kaiser, "Frequency-Coded Chipless RFID Tags: Notch Model, Detection, Angular Orientation, and Coverage Measurements," *Sensors*, vol. 20, no. 7, 2020.

[33] Y. Kato and E. Kato, "Comparison of free-space VNA and TDS measurements using transmission-type frequency selective surfaces," *Microwave and Optical Technology Letters*, vol. 65, no. 8, pp. 2201–2209, 2023.

[34] A. El-Awamry, M. Khaliel, A. Fawky, and T. Kaiser, "A novel multi-tag identification technique for frequency coded chipless RFID systems based on look-up-table approach," in *2017 11th European Conference on Antennas and Propagation (EUCAP)*, 2017, pp. 2070–2074.